GEOPHYSICAL RESEARCH LETTERS, VOL. 40, 5735–5739, doi:10.1002/2013GL058207, 2013

Enhanced cross-shelf exchange by tides in the western Ross Sea

Q. Wang,[1] S. Danilov,[1] H. Hellmer,[1] D. Sidorenko,[1] J. Schröter,[1] and T. Jung[1]

Received 2 October 2013; revised 28 October 2013; accepted 30 October 2013; published 14 November 2013.

[1] The western Ross Sea is one of the key sites for cross-shelf water exchange around Antarctica. The mechanism through which tides affect the cross-shelf exchange in the northwestern Ross Sea is investigated using numerical simulations. Tides are found to increase the high-salinity shelf water (HSSW) outflow through the impact on the warm water intrusion of open ocean origin. The residual tidal currents are onshore along the Modified Circumpolar Deep Water pathway and therefore enhance its intrusion. Lighter ambient water adjacent to the HSSW increases the cross-flow density gradient, thus strengthening the HSSW export. At the same time, the onshore residual current and increased dilution of the HSSW have the potential to reduce the export rate. Owing to the existence of opposite tidal effects, the strongest HSSW export happens at the intermediate tidal forcing strength. The amplification of tides on cross-shelf exchange indicates that the relevant dynamical processes should be simulated or parameterized in climate models in order to adequately predict the ocean.
Citation: Wang, Q., S. Danilov, H. Hellmer, D. Sidorenko, J. Schröter, and T. Jung (2013), Enhanced cross-shelf exchange by tides in the western Ross Sea, *Geophys. Res. Lett.*, *40*, 5735–5739, doi:10.1002/2013GL058207.

1. Introduction

[2] The water mass exchange across the Antarctic continental shelf break is among the key processes that influence the global ocean circulation and ecosystem. Dense, cold shelf water leaves the Antarctic continental shelf and feeds the production of Antarctic Bottom Water (AABW). The latter is an important component of the global meridional overturning circulation and spreads over a large part of the world deep ocean [*Orsi et al.*, 1999, 2002; *Jacobs*, 2004; *Johnson*, 2008]. Warm Circumpolar Deep Water (CDW) from the open ocean can intrude onto the continental shelf at specific locations, carrying heat and nutrients, thus influencing both the heat budget and ecosystem on the shelf [*Prezelin et al.*, 2000; *Dinniman et al.*, 2003]. Recently, it became evident that accelerated onshore heat intrusion from the CDW enhances sub-ice shelf melting and can possibly trigger Antarctic ice sheet mass loss [e.g., *Payne et al.*, 2004; *Jenkins et al.*, 2010; *Jacobs et al.*, 2011]. The important role played by the water mass exchange across the Antarctic shelf break warrants improved understanding of the involved dynamical processes.

[1]Alfred Wegener Institute for Polar and Marine Research, Bremerhaven, Germany.

Corresponding author: Q. Wang, Alfred Wegener Institute for Polar and Marine Research, Bremerhaven 27570, Germany. (qiang.wang@awi.de)

0094-8276/13/10.1002/2013GL058258

[3] With nearly continuous sea ice formation and brine rejection in polynyas in the wintertime, the Ross Sea is one of the major Antarctic marginal seas that export dense shelf water and feed the production of AABW [*Gordon et al.*, 2004; *Whitworth and Orsi*, 2006; *Gordon et al.*, 2009; *Muench et al.*, 2009; *Budillon et al.*, 2011]. Due to the change in the orientation of isobaths along the shelf break, the western Ross Sea is also believed to be a preferable site for CDW onshore intrusions [*Dinniman et al.*, 2003; *Klinck and Dinniman*, 2010]. Recent observations have revealed more details of the warm water intrusion in this region [*Kohut et al.*, 2013].

[4] CDW mixes with the outflowing high-salinity shelf water (HSSW) near the shelf break and produces modified Circumpolar Deep Water (MCDW); the mixing process is significantly enhanced by tides, which are predominantly diurnal with pronounced spring-neap cycles in the western Ross Sea [*Gordon et al.*, 2009; *Padman et al.*, 2009; *Muench et al.*, 2009; *Wang et al.*, 2010]. As shown in these studies, tides not only modify the properties of both outflowing dense shelf water and inflowing warm ambient water near the shelf break through tidal mixing but also strongly modulate the position of the Antarctic Slope Front (ASF) and the descent pathway of dense plumes through tidal advection.

[5] Despite the research efforts mentioned above, the tidal dynamics influencing the HSSW export from the inner shelf to the outer shelf are still unclear. In this study we will explore the interaction between shelf water and MCDW on the continental shelf in the northwestern Ross Sea using numerical simulations. A mechanism through which tides modify the HSSW export rate will be proposed and discussed.

2. Model setup

[6] The model used in this work is the ocean component of the Finite Element Sea ice-Ocean Model (FESOM) [*Wang et al.*, 2013], which was employed to simulate bottom water formation in the Ross and Weddell Seas [*Wang et al.*, 2009, 2010, 2012]. The model domain with variable horizontal mesh resolution used here is 80° wide in longitude (between 130°E and 150°W) and 17° wide in latitude (between 77°S and 60°S). The horizontal mesh resolution changes from 2 km in the western Ross Sea to 30 km outside of it. A resolution of 0.5–1 km is assigned for regions with very steep continental slope, including the shelf break region north of the Drygalski Trough (DT, see Figure 1a for the topography of the northwestern Ross Sea). We use 40 sigma layers in the vertical with refined layer thickness near the bottom.

[7] The model is initialized with the hydrography from the World Ocean Atlas (WOA) 2001 [*Conkright et al.*, 2002]. Because the Ross Sea shelf water is not well represented in the WOA data, we prescribe the initial potential

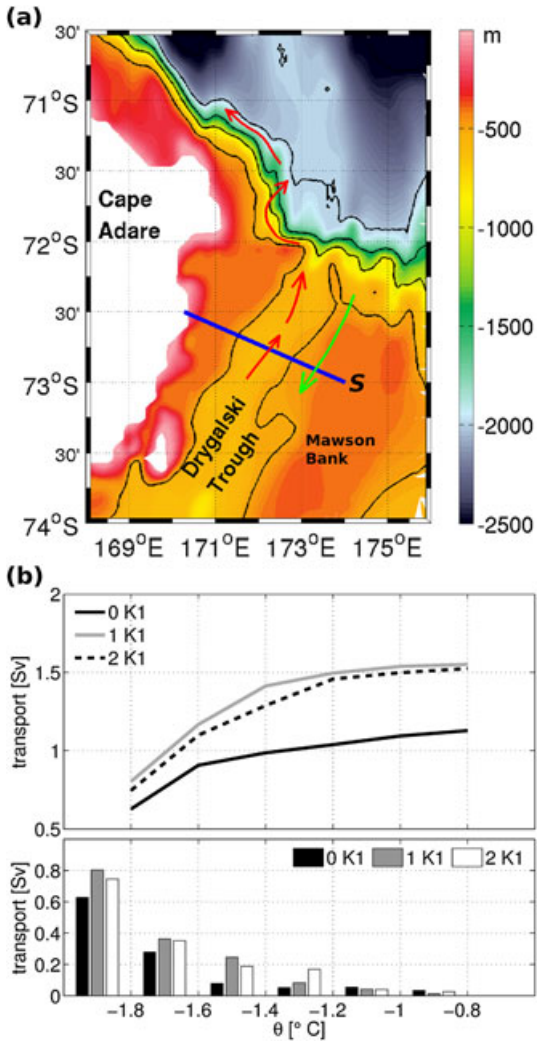

Figure 1. (a) Bathymetry of the western Ross Sea. The red arrows illustrate the export of shelf water and production of AABW, and the green arrow illustrates the open ocean water inflow. The transect *S* discussed in the text is shown by the blue line. Terra Nova Bay (TNB) is located at the southern end of the Drygalski Trough (DT) and not shown in this map. The model domain used in this work is the same as in *Wang et al.* [2010]. (b) The mean HSSW export rates at transect *S* for different temperature classes (bottom) and their cumulative values (top). The transport is classified into six θ classes with an interval of 0.2°C.

temperature and salinity in the DT including the Terra Nova Bay (TNB) based on the AnSlope II CTD data (its section "A" over the shelf, see http://www.ldeo.columbia.edu/res/div/ocp/projects/anslope.shtml). To facilitate the analysis of the model results, a passive tracer with concentration $\tau = 1$ is injected into the HSSW (with salinity in excess of 34.7) in the DT. No atmospheric forcing is applied to generate variability in the HSSW properties; instead, salinity, temperature, and τ south of 74.5°S in the TNB are restored to their initial values during the simulation. More details about the model setup can be found in *Wang et al.* [2010], who showed that this model setup well represents the major tidal dynamics in this region and reproduces AABW formation rates in the range suggested by observations.

[8] The two dominant tidal harmonics in the western Ross Sea are K1 and O1 with similar velocity amplitudes, thus leading to pronounced spring-neap cycles [*Padman et al.*, 2003; *Erofeeva et al.*, 2005; *Robertson*, 2005]. The tidal ellipse magnitudes of the semidiurnal tides are one order of magnitude smaller than the diurnal tides in the northwestern Ross Sea [*Robertson*, 2005], so we will focus on the impact of the diurnal tides in this work. We conducted one simulation without tidal forcing (case 0K1) and the second with the K1 tidal forcing (case 1K1), which is derived from TPXO7.1 [*Egbert and Erofeeva*, 2002] and applied through the open boundaries. In the third experiment (case 2K1), we scaled the K1 tidal forcing magnitude by a factor of 2, resembling the "spring" tidal forcing strength. All experiments were run for 75 days, and the last 20 tidal daily cycles are used for analysis. Two additional experiments, same as 1K1 and 2K1 but with a homogeneous ocean, were conducted to derive the tidal circulation.

3. Model Results

[9] Dense HSSW flows from the DT to the north and feeds the production of AABW which escapes the Ross Sea along the deep slope to the northwest [*Gordon et al.*, 2009]. The focus of this work is the dynamics of outflowing HSSW on the continental shelf and its interaction with the MCDW inflow. Figure 1b shows the temporal mean of the HSSW export rates at transect *S* shown in Figure 1a. The HSSW is defined with $\tau \geq 0.1$ and salinity $S \geq 34.7$ hereafter. Both the individual HSSW transports for different temperature classes and the cumulative values are shown. The total transport (for all the HSSW with potential temperature $\theta \leq -0.8$°C) is the lowest in case 0K1. It is the highest in case 1K1, about 36% higher than in case 0K1 and only slightly higher than in case 2K1. For all the low-temperature components ($\theta \leq -1.2$°C), case 0K1 has smaller export rates than the other two cases.

[10] Figure 2 shows the mean temperature, salinity, velocity, and potential density (σ_θ) at transect *S*. The transect is slightly south of the trough sill, where the tidal current cannot advect MCDW directly from the shelf break. The dense HSSW flows offshore to the north along the western flank of the DT in all three cases. The bottom intensified outflow velocity is associated with the coldest and most saline HSSW originating from the TNB. The warm MCDW flows onshore on the eastern side of the outflow, along the western slope of the Mawson Bank. Observations identified the western slope of the Mawson Bank as one of the major intrusion pathways of MCDW onto the Ross Sea continental shelf [*Kohut et al.*, 2013].

[11] The inflow at this transect is the warmest in case 0K1, indicating that tides in cases 1K1 and 2K1 have increased the mixing of the warm open ocean water with cold shelf water at the outer shelf, as found in previous observational and modeling studies [*Whitworth and Orsi*, 2006; *Muench et al.*, 2009; *Padman et al.*, 2009; *Wang et al.*, 2010]. The increased mixing at the outer shelf due to tides is also shown by the $\tau = 0.1$ contour line at transect *S* (Figure 2). In case 2K1 the inflowing MCDW contains a much larger portion of HSSW entrained at the outer shelf.

[12] Consistent with the HSSW export transport, the outflow velocity is the largest in case 1K1 and smallest in case 0K1 (Figure 2b). The mean export velocity averaged

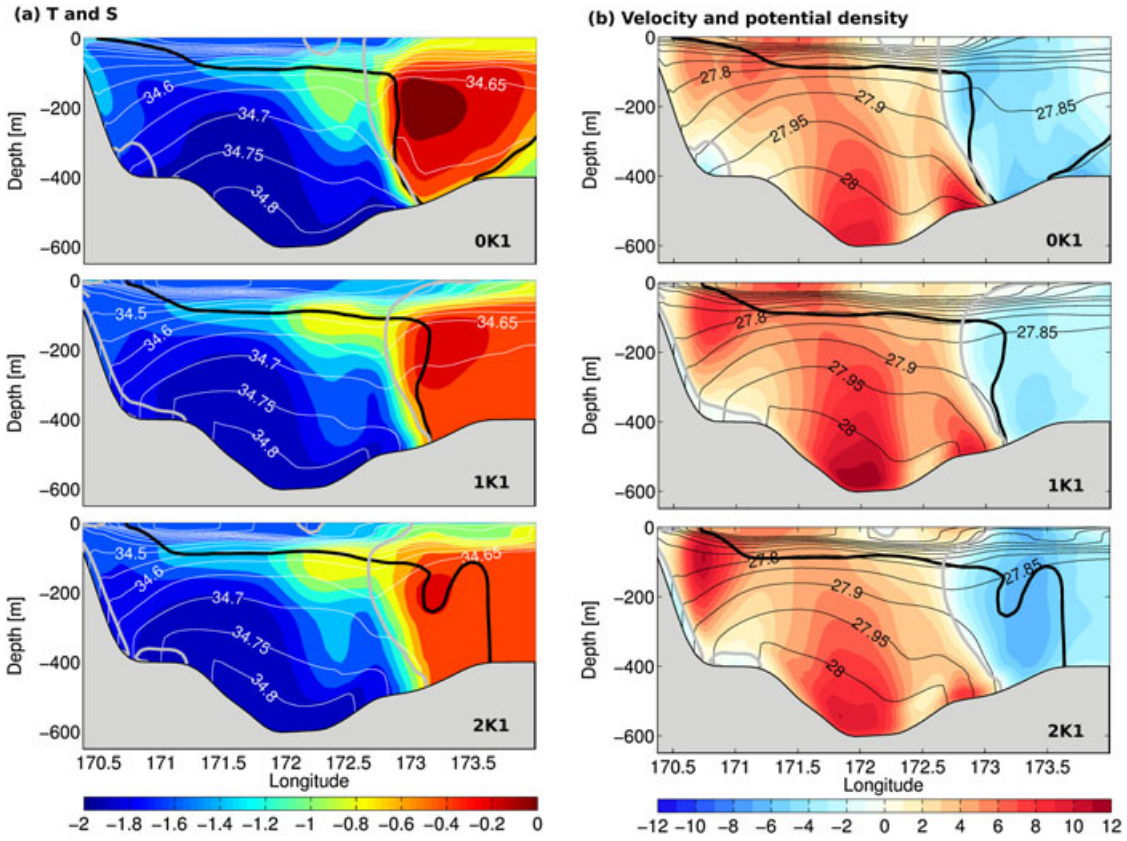

Figure 2. (a) Mean potential temperature (°C, color) and salinity (white contour lines) in the transect *S* shown in Figure 1a. (b) Mean velocity normal to the transect (cm/s, color) and potential density σ_θ (kg/m^3, contour lines). Offshore velocity (export) is positive. The location where the passive tracer $\tau = 0.1$ is shown by the thick black line. The zero velocity contour lines are shown by thick gray lines. The transect direction is chosen to be approximately perpendicular to the mean export velocity in order to show its magnitude.

over the HSSW transect is 3.6cm/s, 5.7cm/s, and 4.9cm/s for cases 0K1, 1K1, and 2K1, respectively. The largest near-bottom velocity in the core of the outflow is associated with the strongest along-transect density gradient, showing the typical structure of geostrophic density currents in a trough. In all three cases there is a light, relatively warm subsurface layer on the top right side of the outflowing HSSW, which thins from the east side of the trough to the west (Figure 2a). In contrast to the MCDW inflow, the temperature of this subsurface warm layer is the lowest in case 0K1 and highest in case 2K1 (Figures 2a and 3).

4. Discussion

[13] The geostrophic velocity of the outflow is controlled by the cross-trough density and hydrostatic pressure gradient between the dense shelf water and light ambient water. Modifications in the light warm water adjacent to the dense shelf water can therefore influence the shelf water outflow strength [*Kida*, 2011; *Wang et al.*, 2012]. We calculated the HSSW export rate based on the geostrophic velocity diagnosed from the temperature and salinity along transect *S*. The surface velocity from the simulations is used as the surface boundary condition. The corresponding barotropic tidal velocity obtained from the homogeneous ocean simulations is subtracted from the surface velocity in cases 1K1 and 2K1 in the calculation. The diagnosed HSSW transport is 1.06 sverdrup (Sv) in case 0K1 and 1.63 Sv in case 1K1. The enhancement in the outflow in case 1K1 is expected from the warmer subsurface layer adjacent to the HSSW than in case 0K1 (Figures 2 and 3). In case 2K1 the subsurface warm layer extends deeper and more westward, and the diagnosed HSSW transport using the geostrophic velocity increases to 1.8 Sv.

[14] To understand the role of tides on the cross-shelf exchange, we calculated the temporal mean barotropic velocity normal to transect *S* for the two tidal simulations with a homogeneous ocean (Figure 4). It represents the tidal residual current (rectified flow). The velocity patterns are similar in the two simulations but with different magnitudes. Except for the small region near the coast (170.7°E), there is no offshore residual current in the DT. The strongest residual currents are onshore and along the western slope of the Mawson Bank (173.3°E), which tend to strengthen the MCDW intrusion. The onshore heat flux referenced to the potential temperature –0.8°C for the region 173°E to 174°E at transect *S* is 1 TW, 1.3 TW, and 2.1 TW for cases 0K1, 1K1, and 2K1, respectively. Although the inflow potential temperature decreases with increasing tidal forcing, tidal currents increase the heat flux.

[15] The core of the HSSW outflow coincides with the location of the weakest residual currents (at about 171.5–172°E; see Figure 2), but the onshore residual currents still have effects to reduce the HSSW outflow in the two

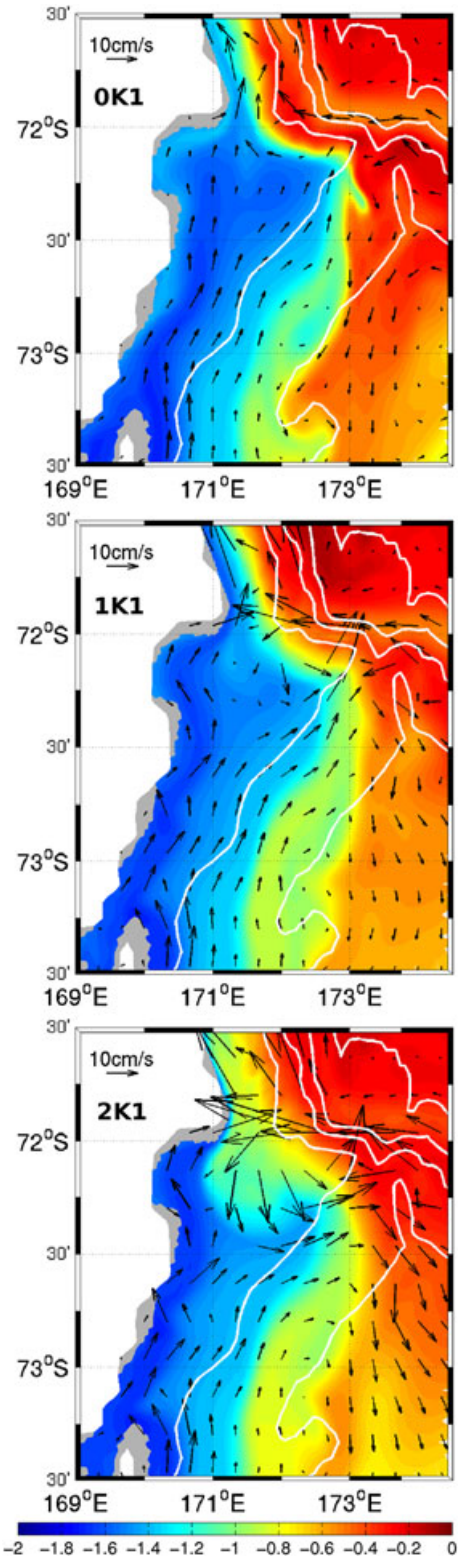

Figure 3. Mean potential temperature (color patch) and velocity (arrows) at 100 m depth.

simulations with tides. If we calculate the HSSW transport using the geostrophic balance without subtracting the barotropic tidal velocity, the HSSW export transport is 1.52 Sv and 1.49 Sv in cases 1K1 and 2K1, respectively. These estimated values are close to the exact ones computed directly from the model velocity (Figure 1b). Although the geostrophic HSSW outflow is stronger in case 2K1 than in case 1K1, the onshore residual currents make the net HSSW outflow in case 2K1 slightly weaker than in case 1K1.

[16] It has been speculated that tides may increase the export of HSSW from the DT through the offshore movement of the ASF [*Whitworth and Orsi*, 2006]. However, the enhancement of HSSW export associated with the offshore tidal advection could be compensated by the reduction associated with the onshore tidal advection occurring in the opposite phase during the tidal cycle. Here we propose a different mechanism through which tides can enhance the cross-shelf water exchange. Residual tidal currents increase the MCDW intrusion. Due to the close proximity to the HSSW outflow, it increases the cross-trough density and hydrostatic pressure gradient. This leads to the enhancement of the HSSW export. At the same time the onshore tidal residual currents tend to reduce the HSSW export, and the strongest export happens at intermediate tidal forcing strength. An extra experiment was carried out with both the K1 and O1 constituents, which have similar velocity magnitudes and lead to spring-neap cycles. In this realistic situation the residual tidal currents at transect *S* are found to be similar to the case 1K1 and tides do increase the HSSW export compared to the case without tides (not shown).

[17] In addition to the two competing tidal effects discussed above, there is another important process that can influence the HSSW export. With increasing MCDW intrusion, the HSSW layer gets more diluted in the DT. This effect has the potential to reduce the HSSW export. The HSSW transport based on the geostrophic velocity increases by 0.57 Sv from case 0K1 (1.06 Sv) to case 1K1 (1.63 Sv). However, the transport in case 2K1 (1.8 Sv) is higher than in case 1K1 by only 0.17 Sv. This is consistent with the stronger dilution of the HSSW in case 2K1 (Fig. 2). The increase in the geostrophic HSSW transport is relatively small from case 1K1 to case 2K1, so the increased onshore residual currents can readily reduce the net HSSW export in case 2K1 to the level as in case 1K1.

[18] In the above discussion we ignored the interaction of barotropic and baroclinic tides and used the tidal velocity from the homogeneous tidal model in the calculation. Considering the dominance of the barotropic component in

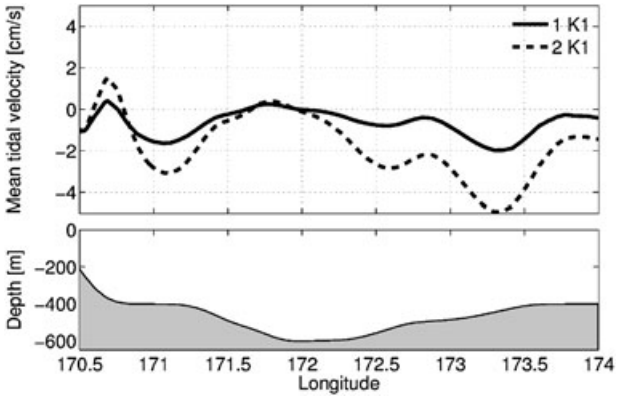

Figure 4. (top) Tidal residual velocity (cm/s) normal to the transect *S* shown in Figure 1a. Positive values indicate offshore flow. (bottom) The ocean bathymetry along the transect.

tidal velocity, the general conclusion is expected to be valid. In this work we also ignored the variability in the HSSW characteristics and restored the temperature and salinity in TNB. Such an idealized setup facilitates the illustration of the dynamical processes discussed here. However, other important processes, such as those related to wind forcing [*Fusco et al.*, 2009], icebergs [*Dinniman et al.*, 2007], and tidal mixing near the critical latitude of the semidiurnal tides, have to be explored and considered together in ocean general circulation modeling in the future effort.

5. Conclusion

[19] In this study we used numerical simulations to elucidate the impact of tides on the interaction between the HSSW outflow and MCDW inflow in the northwestern Ross Sea. The mechanism through which tides increase the HSSW export is proposed and discussed. Tides enhance the MCDW intrusion through rectified tidal currents along the western slope of the Mawson Bank; increased relatively light water adjacent to the HSSW then enhances the geostrophic outflow. The onshore tidal residual current and the dilution of the HSSW layer have the potential to reduce the HSSW export rate. Therefore, tides have opposite effects competing with each other. For realistic tidal forcing with two major diurnal constituents, the positive effect dominates and the HSSW export from the inner shelf to the outer shelf is enhanced.

[20] The northwestern Ross Sea is one of the key sites for cross-shelf water exchange around Antarctica; tides significantly enhance this exchange process. The dynamical processes studied in this work are not adequately represented in large-scale ocean modeling, and their improved representation in climate models is warranted. This study also indicates that designing observation systems should take both the onshore and offshore processes together into account to better understand and monitor the ocean changes in this region.

[21] **Acknowledgments.** The authors thank the two anonymous reviewers for their helpful comments. The computational resources for this work were provided through the North-German Supercomputing Alliance (HLRN). Part of the financial support is provided by the REKLIM initiative.

[22] The Editor thanks two anonymous reviewers for their assistance in evaluating this paper.

References

Budillon, G., P. Castagno, S. Aliani, G. Spezie, and L. Padman (2011), Thermohaline variability and Antarctic bottom water formation at the Ross Sea shelf break, *Deep Sea Res. I*, *58*, 1002–1018.

Conkright, M., R. A. Locarnini, H. Garcia, T. O'Brien, T. Boyer, C. Stephens, and J. Antonov (2002), *World Ocean Atlas 2001: Objective Analyses, Data Statistics, and Figures, CD-ROM Documentation*, 17 pp., National Oceanographic Data Center, Silver Spring, MD.

Dinniman, M. S., J. M. Klinck, and W. O. Smith (2003), Cross-shelf exchange in a model of the Ross Sea circulation and biogeochemistry, *Deep Sea Res. II*, *50*, 3103–3120.

Dinniman, M. S., J. M. Klinck, and W. O. Smith (2007), Influence of sea ice cover and icebergs on circulation and water mass formation in a numerical circulation model of the Ross Sea, Antarctica, *J. Geophys. Res.*, *112*, C11013, doi:10.1029/2006JC004036.

Egbert, G. D., and S. Y. Erofeeva (2002), Efficient inverse modeling of barotropic ocean tides, *J. Atmos. Oceanic Technol.*, *19*, 183–204.

Erofeeva, S. Y., L. Padman, and G. Egbert (2005), Assimilation of ship-mounted ADCP data for barotropic tides: Application to the Ross Sea, *J. Atmos. Oceanic Technol.*, *22*, 721–734.

Fusco, G., G. Budillon, and G. Spezie (2009), Surface heat fluxes and thermohaline variability in the Ross Sea and in Terra Nova Bay polynya, *Cont. Shelf Res.*, *29*, 1887–1895.

Gordon, A. L., E. Zambianchi, A. Orsi, M. Visbeck, C. F. Giulivi, T. Whitworth, and G. Spezie (2004), Energetic plumes over the western Ross Sea continental slope, *Geophys. Res. Lett.*, *31*, L21302, doi:10.1029/2004GL020785.

Gordon, A. L., A. H. Orsi, R. Muench, B. A. Huber, E. Zambianchi, and M. Visbeck (2009), Western Ross Sea continental slope gravity currents, *Deep Sea Res. II*, *56*, 796–817.

Jacobs, S. S. (2004), Bottom water production and its links with the thermohaline circulation, *Antarct. Sci.*, *16*, 427–437.

Jacobs, S. S., A. Jenkins, C. F. Giulivi, and P. Dutrieux (2011), Stronger ocean circulation and increased melting under Pine Island Glacier ice shelf, *Nat. Geosci.*, *4*, 519–523.

Jenkins, A., K. W. Nicholls, and H. F. J. Corr (2010), Observation and parameterization of ablation at the base of Ronne Ice Shelf, Antarctica, *J. Phys. Oceanogr.*, *40*, 2298–2312.

Johnson, G. C. (2008), Quantifying Antarctic bottom water and North Atlantic deep water volumes, *J. Geophys. Res.*, *113*, C05027, doi:10.1029/2007JC004477.

Kida, S. (2011), The impact of open oceanic processes on the Antarctic bottom water outflows, *J. Phys. Oceanogr.*, *41*, 1941–1957.

Klinck, J. M., and M. S. Dinniman (2010), Exchange across the shelf break at high southern latitudes, *Ocean Sci.*, *6*, 513–524.

Kohut, J., E. Hunter, and B. Huber (2013), Small-scale variability of the cross-shelf flow over the outer shelf of the Ross Sea, *J. Geophys. Res. Oceans*, *118*, 1863–1876, doi:10.1002/jgrc.20090.

Muench, R., L. Padman, A. Gordon, and A. Orsi (2009), A dense water outflow from the Ross Sea, Antarctica: Mixing and the contribution of tides, *J. Mar. Syst.*, *77*, 369–387.

Orsi, A. H., G. C. Johnson, and J. L. Bullister (1999), Circulation, mixing, and production of Antarctic Bottom Water, *Prog. Oceanogr.*, *43*, 55–109.

Orsi, A. H., W. M. Smethie, and J. L. Bullister (2002), On the total input of Antarctic waters to the deep ocean: A preliminary estimate from chlorofluorocarbon measurements, *J. Geophys. Res.*, *107* (C8), 3122, doi:10.1029/2001JC000976.

Padman, L., S. Erofeeva, and I. Joughin (2003), Tides of the Ross Sea and Ross Ice Shelf cavity, *Antarct. Sci.*, *15*, 31–40.

Padman, L., S. L. Howard, A. H. Orsi, and R. D. Muench (2009), Tides of the northwestern Ross Sea and their impact on dense outflows of Antarctic bottom water, *Deep Sea Res. II*, *56*, 818–834.

Payne, A. J., A. Vieli, A. P. Shepherd, D. J. Wingham, and E. Rignot (2004), Recent dramatic thinning of largest West Antarctic ice stream triggered by oceans, *Geophys. Res. Lett.*, *31*, L23401, doi:10.1029/2004GL021284.

Prezelin, B. B., E. E. Hofmann, C. Mengelt, and J. M. Klinck (2000), The linkage between Upper Circumpolar Deep Water (UCDW) and phytoplankton assemblages on the west Antarctic Peninsula continental shelf, *J. Mar. Res.*, *58*, 165–202.

Robertson, R. (2005), Baroclinic and barotropic tides in the Ross Sea, *Antarct. Sci.*, *17*, 107–120.

Wang, Q., S. Danilov, and J. Schröter (2009), Bottom water formation in the southern Weddell Sea and the influence of submarine ridges: Idealized numerical simulations, *Ocean Modell.*, *28*, 50–59.

Wang, Q., S. Danilov, H. Hellmer, and J. Schröter (2010), Overflow dynamics and bottom water formation in the western Ross Sea: The influence of tides, *J. Geophys. Res.*, *115*, C10054, doi:10.1029/2010JC006189.

Wang, Q., S. Danilov, E. Fahrbach, J. Schröter, and T. Jung (2012), On the impact of wind forcing on the seasonal variability of Weddell Sea Bottom Water transport, *Geophys. Res. Lett.*, *39*, L06603, doi:10.1029/2012GL051198.

Wang, Q., S. Danilov, D. Sidorenko, R. Timmermann, C. Wekerle, X. Wang, T. Jung, and J. Schröter (2013), The Finite element sea ice-ocean model (FESOM): Formulation of an unstructured-mesh ocean general circulation model, *Geosci. Model Dev. Discuss.*, *6*, 3893–3976.

Whitworth, T., and A. H. Orsi (2006), Antarctic bottom water production and export by tides in the Ross Sea, *Geophys. Res. Lett.*, *33*, L12609, doi:10.1029/2006GL026357.